

DOI: 10.1002/cphc.201301232

# Spatially Selective Heteronuclear Multiple-Quantum Coherence Spectroscopy for Biomolecular NMR Studies

Bharathwaj Sathyamoorthy,<sup>[a, c]</sup> David M. Parish,<sup>[a]</sup> Gaetano T. Montelione,<sup>[b]</sup> Rong Xiao,<sup>[b]</sup> and Thomas Szyperski<sup>\*[a]</sup>

Spatially selective heteronuclear multiple-quantum coherence (SS HMQC) NMR spectroscopy is developed for solution studies of proteins. Due to “time-staggered” acquisition of free induction decays (FIDs) in different slices, SS HMQC allows one to use long delays for longitudinal nuclear spin relaxation at high repetition rates. To also achieve high intrinsic sensitivity, SS HMQC is implemented by combining a single spatially selec-

tive <sup>1</sup>H excitation pulse with nonselective <sup>1</sup>H 180° pulses. High-quality spectra were obtained within 66 s for a 7.6 kDa uniformly <sup>13</sup>C,<sup>15</sup>N-labeled protein, and within 45 and 90 s for, respectively, two proteins with molecular weights of 7.5 and 43 kDa, which were uniformly <sup>2</sup>H,<sup>13</sup>C,<sup>15</sup>N-labeled, except for having protonated methyl groups of isoleucine, leucine and valine residues.

## 1. Introduction

The ever-increasing sensitivity of NMR spectrometers<sup>[1]</sup> has fostered the development of a large number of approaches for rapidly acquiring multidimensional NMR spectra.<sup>[2]</sup> In turn, this has enabled researchers to obtain the information they seek more rapidly. For example, NMR-based structural and dynamic atomic-resolution studies can be pursued with reduced demand for spectrometer time,<sup>[3]</sup> and time-resolved studies can be designed with higher time resolution—faster processes have become amenable to “real time” observations using NMR.<sup>[4]</sup>

Three- and higher-dimensional spectra can be acquired rapidly by jointly sampling two or more indirect evolution periods using reduced-dimensionality<sup>[5]</sup> (RD), or G-matrix Fourier-transform (GFT) projection NMR<sup>[6]</sup> along with its derivatives “projection reconstruction” and “automated projection NMR spectroscopy”.<sup>[7]</sup> Other approaches can be employed even for the single indirect dimension in 2D NMR spectroscopy. These include: 1) non-uniform or severely truncated time-domain sampling combined with non-Fourier-transform-based spectral processing<sup>[8]</sup> (maximum entropy, multi-dimensional decomposi-

tion, compressed sensing, covariance processing); 2) longitudinal relaxation optimization (L-optimization),<sup>[9]</sup> allowing for a significant reduction of the relaxation delay between scans; 3) Hadamard spectroscopy,<sup>[10]</sup> relying on the use of arrays of selective radio-frequency (RF) pulses with relative signs as encoded in Hadamard matrices; 4) ultrafast NMR,<sup>[4b]</sup> where chemical shift evolution in the indirect dimension is spatially encoded such that frequency domain signals can be obtained by applying a “read-out” pulsed field gradient (PFG) during signal detection in the direct dimension.


The development of ultrafast NMR, which relies on spatio-temporal encoding of the evolution of indirect chemical shifts followed by their repetitive decoding/re-encoding during signal detection in the direct dimension, has allowed recording of multidimensional spectra in a single scan. The utility of ultrafast NMR stimulated the implementation of a variety of other experiments, based on the fact that RF pulses become spatially selective when applied concomitantly with PFGs of suitable strength. The major challenges associated with ultrafast NMR arise from the necessity to apply “read-out PFGs” during signal detection: this greatly reduces intrinsic sensitivity and can also affect line shapes.

Therefore, NMR experiments were developed that allow the use of read-out PFGs to be avoided, but which take advantage of spatially selective excitation. It is possible to design RF-pulse phase cycles such that the receiver phase is the same for all steps of a phase cycle. All steps of the phase cycle can then be employed simultaneously in different “slices” of the sample and the detected signal simply represents the desired sum of all free induction decays (FIDs) associated with the phase-cycling scheme; read-out PFGs are not required. This approach has been named simultaneously cycled (SC) NMR spectroscopy.<sup>[11]</sup> Furthermore, the signal arising from different slices can be detected separately using “time-staggered” excitation (Figure 1), that is, only fractions of the sample volume are used

[a] Dr. B. Sathyamoorthy, Dr. D. M. Parish, Prof. T. Szyperski  
Department of Chemistry  
The State University of New Jersey at Buffalo  
Buffalo NY 14260 (USA)  
E-mail: szypersk@buffalo.edu

[b] Prof. G. T. Montelione, Dr. R. Xiao  
Department of Molecular Biology and Biochemistry  
and Robert Wood Johnson Medical School, Rutgers  
The State University of New Jersey  
Piscataway, NJ 08854 (USA)

[c] Dr. B. Sathyamoorthy  
Present address: Department of Biophysics and Chemistry  
University of Michigan  
Ann Arbor, MI 48108 (USA)

 Supporting Information for this article is available on the WWW under <http://dx.doi.org/10.1002/cphc.201301232>.

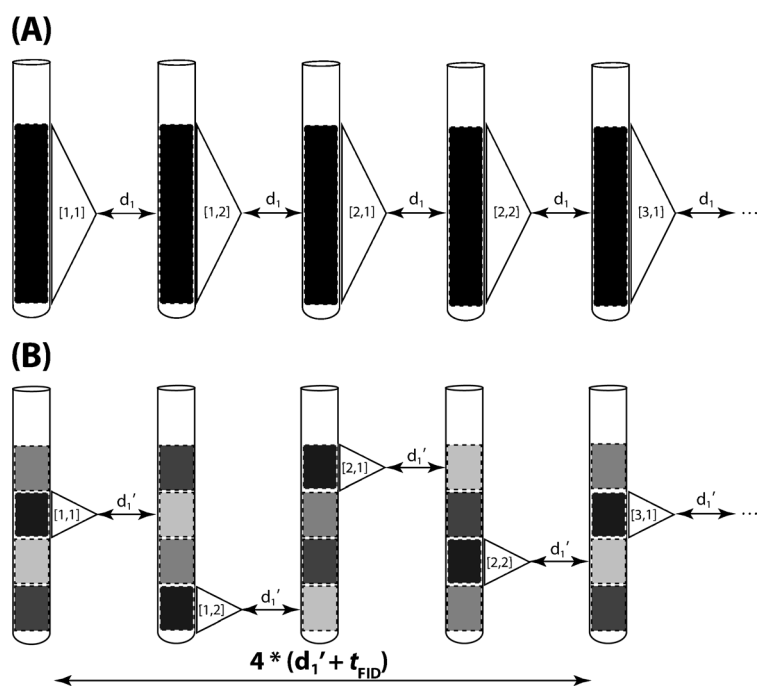


**Figure 1.** Comparison of conventional with time-staggered data acquisition relying on spatial excitation. A) Conventional data acquisition: the entire sample volume within the RF-detection coil is utilized to record FIDs with a relaxation delay  $d_1$  between scans. Black represents the excited region of the sample where a sizable steady-state magnetization is present before excitation and for which the signal is detected. The FID is represented by a triangle and  $[N,P]$  within this indicates the real data point  $N$  and corresponding phase-cycling step  $P$  for the indirect dimension. As an example, complex data acquisition ( $N=1,2$ ) is combined with a two-step phase cycle ( $P=1,2$ ) cycle for axial peak suppression.<sup>[12]</sup> B) Time-staggered data acquisition relying on spatial excitation of one slice of the entire volume at a time defining the region for which an FID is detected. Considering  $t_{\text{FID}}$  as the time required to detect an FID and  $d_1'$  as the relaxation delay between scans, the same steady-state magnetization exists as in (A) if  $d_1 + t_{\text{FID}} = 4(d_1' + t_{\text{FID}})$ . The transitions from pale gray to gray, then to dark gray and eventually to black (second slice from the top) indicates progressing longitudinal relaxation in a slice while other slices are excited. As a result, NMR time-domain data can be acquired more rapidly while ensuring that sufficiently long relaxation times between scans are used.

to acquire the FIDs for a multidimensional experiment,<sup>[13]</sup> or to measure accurately nuclear spin relaxation times<sup>[14]</sup> or molecular translational diffusion.<sup>[15]</sup> For the design of new experiments, it is important to note that the intrinsic sensitivity of a spatially selective (SS) NMR experiment is significantly reduced by each additional SS RF pulse, and also that the SS  $180^\circ$  pulses required for refocusing shift evolution introduce large phase shifts, which are rather difficult to compensate for, in addition to the significant loss of sensitivity. It is thus desirable to implement a given experiment with the least possible number of such pulses, ideally with a single SS RF pulse for excitation.

Furthermore, longitudinal spin relaxation between scans greatly affects the intrinsic sensitivity of an NMR experiment: sensitivity per unit time is maximal when the total time for longitudinal relaxation between scans is about  $1.25 T_1$  (where  $T_1$  represents the corresponding  $^1\text{H}$  relaxation time). Therefore,  $L$ -optimization,<sup>[2a,6b,9,16]</sup> possibly combined with the application of an excitation pulse at the “Ernst angle”,<sup>[4h,17]</sup> is advantageous whenever rapid sampling is accomplished by shortening the

relaxation delay between scans. Furthermore, quantitative analysis of NMR spectra when, for example, measuring relative concentrations or deriving distance information from nuclear Overhauser effects, can be severely impeded by short relaxation delays (which lead to significantly different steady-state magnetizations for nuclear spins exhibiting different  $T_1$  relaxation). Therefore, “time-staggered” acquisition of FIDs (Figure 1) from selectively excited slices offers the distinct advantage of sampling FIDs rapidly while using a sufficiently long relaxation delay between scans. This becomes particularly important whenever  $L$ -optimization is not feasible, for example, in deuterated systems<sup>[18]</sup> or when protein spectra are acquired in  $\text{D}_2\text{O}$ . In both cases,  $^1\text{H}$ – $^1\text{H}$  dipolar interactions that promote longitudinal relaxation are removed which results in longer  $^1\text{H}$   $T_1$  relaxation times.

Polypeptide  $^{15}\text{N}$ – $^1\text{H}$  and methyl group  $^{13}\text{C}$ – $^1\text{H}$  2D chemical shift correlation experiments are widely used to study the polypeptide backbone and core of a protein, respectively. Heteronuclear multiple-quantum coherence (HMQC) NMR<sup>[19]</sup> spectroscopy relies on only two  $^1\text{H}$  RF pulses and thus offers itself for implementation of SS versions. Here we present HMQC experiments that combine a single SS  $90^\circ$   $^1\text{H}$  pulse with two nonselective  $^1\text{H}$   $180^\circ$  pulses such that  $^1\text{H}$  magnetization outside of the selectively excited slice is returned to the  $z$ -axis before signal detection. Specifically, we implemented simultaneous<sup>[20]</sup> 2D [ $^{13}\text{C}^{\text{methyl}}/^{15}\text{N}$ ,  $^1\text{H}$ ] HMQC (sim-HMQC) and constant time (CT)<sup>[21]</sup> [ $^{13}\text{C}^{\text{methyl}}, ^1\text{H}$ ] HMQC (CT-HMQC). Applications of sim-HMQC are presented for U- $[^{13}\text{C}, ^{15}\text{N}]$  ubiquitin (7.6 kDa) as well as for the U- $[^2\text{H}, ^{13}\text{C}, ^{15}\text{N}]$ -labeled Northeast Structural Genomics Consortium (NESG; <http://www.nesg.org>) target GmR137 (7.5 kDa) in which the methyl groups of isoleucine, leucine, valine are protonated (“ILV-protonated”).<sup>[22]</sup> The application of CT-HMQC is demonstrated for U- $[^2\text{H}, ^{13}\text{C}, ^{15}\text{N}]$ -labeled, ILV methyl protonated, maltose-binding protein (MBP, 43.4 kDa) because methyl HMQC for large proteins benefits greatly from a “transverse relaxation-optimized spectroscopy (TROSY) effect”<sup>[23]</sup> arising from (partial) cancellation of  $^{13}\text{C}$ – $^1\text{H}$  dipolar relaxation within the methyl groups.

## Experimental Section

### NMR Samples

NMR data were acquired for three samples: 1) U- $[^{13}\text{C}, ^{15}\text{N}]$ -labeled ubiquitin [7.6 kDa; 3.7 mM in  $\text{H}_2\text{O}/\text{D}_2\text{O}$  (9:1 v/v), containing sodium phosphate buffer (50 mM, pH 6.0) and 0.02%  $\text{NaN}_3$ ], 2) U- $[^2\text{H}, ^{13}\text{C}, ^{15}\text{N}]$ -labeled, ILV methyl protonated, NESG target GmR137 (7.5 kDa; 0.7 mM in  $\text{H}_2\text{O}/\text{D}_2\text{O}$  (9:1 v/v), containing 2-( $N$ -morpholino)ethanesulfonic acid (20 mM, pH 6.5), 0.02%  $\text{NaN}_3$ , DTT (10 mM),  $\text{CaCl}_2$  (5 mM),  $\text{NaCl}$  (200 mM)], and 3) U- $[^2\text{H}, ^{13}\text{C}, ^{15}\text{N}]$ -labeled, ILV methyl protonated MBP (43.4 kDa) complexed to  $\beta$ -cyclodextrin<sup>[24]</sup> (1 mM in the same buffer as sample 2).

## NMR Data Acquisition and Analysis

NMR experiments were performed at 25 °C for ubiquitin and at 20 °C for GmR137 and MBP using a Varian INOVA 750 MHz spectrometer equipped with a cryogenic  $^1\text{H}[^{13}\text{C},^{15}\text{N}]$  probe (Table S1 in the Supporting Information). The maximum available z axis PFG amplitude was  $G_z = 52 \text{ Gcm}^{-1}$ . NMR data were processed using the software NMRPipe<sup>[25]</sup> and analyzed using the program SPARKY (T. D. Goddard and D. G. Kneller, SPARKY 3, University of California, San Francisco, CA). Polypeptide backbone amide and methyl  $^1\text{H}$   $T_1$  relaxation times were determined by fitting a mono-exponential function of the signal-to-noise ratio ( $S/N$ ) as a function of the relaxation delays (300, 400, 500, 600, 700, 900, 1100, 1300, 1600, 2100, 4100 and 5100 ms) employed for a series of heteronuclear single-quantum coherence (HSQC) spectra.

## Spatially Selective HMQC

To enhance intrinsic sensitivity, sim-HMQC (Figure 2A) and CT-HMQC (Figure 2B) were implemented by combining a single spatially selective  $90^\circ$   $^1\text{H}$  pulse (Figure 3) with two nonselective  $180^\circ$   $^1\text{H}$  pulses such that  $^1\text{H}$  magnetization outside of the selectively excited slice was returned to the z axis in the middle of the indirect chemical shift evolution (Figure 4). This allows one to avoid an SS  $180^\circ$   $^1\text{H}$  pulse that would result in a significant loss of sensitivity resulting from the application PFGs in the presence of transverse magnetization. Moreover, because two-spin coherence is generated in HMQC starting from  $^1\text{H}$  steady-state magnetization, all  $^{15}\text{N}/^{13}\text{C}$  pulses can likewise be nonselective.

Spatially (i.e. slice) selective excitation was accomplished using an RF pulse with the shape of the three central lobes of a sinc function as previously described.<sup>[11]</sup> In brief, the time-bandwidth product<sup>[26]</sup> (i.e. the product of pulse width  $pw$  and excited spectral width  $bw$ ) of such a pulse is 6. For a given amplitude of  $G_z = 27 \text{ Gcm}^{-1}$  of the magnetic z-field gradient (about one half of the maximum possible amplitude of the gradient amplifier used for the present study) which is applied simultaneously with the RF pulse and the gyromagnetic ratio of protons  $\gamma_{\text{H}} = 4.258 \text{ kHzG}^{-1}$ , a given slice thickness  $\Delta z$  requires that the RF pulse excites a width of  $bw = \Delta z G_z \gamma_{\text{H}}$ . For the probe used in this study, the length of the sample volume located within the RF coil is 16 mm along the z axis. However, measurement of SS 1D  $^1\text{H}$  spectra revealed that significant imperfections of the PFGs in the upper  $\sim 4$  mm prevented the acquisition of high-quality spectra. Hence, we decided to choose four slices with  $\Delta z = 3.0$  mm for implementing SS HMQC as shown in Figure 3B (thereby excluding the upper  $\sim 4$  mm). With  $\Delta z = 3.0$  mm, one obtains  $bw = 33.3 \text{ kHz}$  (which is also equal to the shift of the carrier position when switching from one slice to a neighboring one) and  $pw = 180 \mu\text{s}$  is required for the selective excitation. To compensate for chemical shift evolution during the application of the selective pulse, a “re-phasing” PFG<sup>[11]</sup> was applied, with half the duration of the selective pulse, immediately after the RF pulse (Figure 3A). The amplitude of this gradient was tuned experimentally by maximizing the signal intensities observed in SS 1D  $^1\text{H}$  NMR spectra.

## Intrinsic Sensitivity of SS Versus Conventional HMQC

The signal intensity  $S$  detected for a slice is proportional to its thickness  $\Delta z$ , whereas the noise  $N$  remains the same: signal detection is accomplished using an RF coil that extends over the entire volume within a detection coil of length  $l$  in the z-direction. Importantly, however, if  $n$  slices are used for SS HMQC,  $n$  FIDs can be acquired within the same time that is required to acquire a single

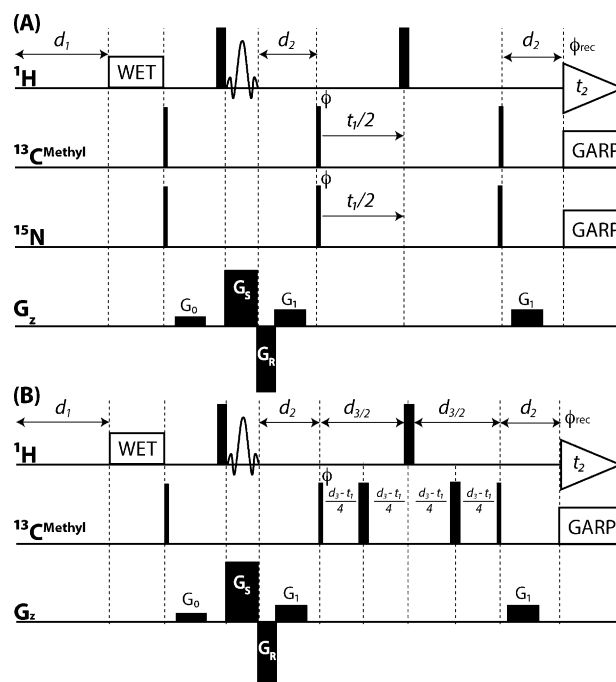


**Figure 2.** SS HMQC RF-pulse schemes implemented for  $n=4$  slices. Rectangular  $90^\circ$  and  $180^\circ$  pulses are indicated by thin and thick vertical bars, respectively, and the phase  $\phi$  of the excitation pulses are indicated. When no RF phase is marked, the pulse is applied along the x-axis. High-power  $90^\circ$  pulse lengths are: 8.5  $\mu\text{s}$  for  $^1\text{H}$ , 15.5  $\mu\text{s}$  for  $^{13}\text{C}$  and 39.0  $\mu\text{s}$  for  $^{15}\text{N}$ . The length of the three-lobed sinc pulse for SS excitation is 180  $\mu\text{s}$  and the concomitantly applied SS PFG  $G_s$  has an amplitude of  $27 \text{ Gcm}^{-1}$ . The re-phasing PFG  $G_R$  has an amplitude of  $31 \text{ Gcm}^{-1}$  and a duration of 90  $\mu\text{s}$ . Water suppression enhanced through  $T_1$ -effects (WET)<sup>[12]</sup> is employed to suppress the water signal. A globally optimized alternating phase rectangular pulse (GARP) sequence<sup>[26]</sup> is used for decoupling of  $^{13}\text{C}$  (RF field strength = 2.0 kHz) and  $^{15}\text{N}$  (RF field strength = 1.5 kHz) during acquisition of the FIDs. The  $^1\text{H}$ ,  $^{13}\text{C}$  and  $^{15}\text{N}$  carrier positions are set to  $\delta = 4.78$ , 20.0 and 118.0 ppm, respectively. Sampling in  $t_1$  ( $^{13}\text{C}/^{15}\text{N}$ ) starts at half increments to ensure a  $180^\circ$  first-order phase correction. The duration and strengths of the rectangular PFGs are  $G_0$  (0.5 ms, 3.2  $\text{Gcm}^{-1}$ ) and  $G_1$  (0.5 ms, 6.3  $\text{Gcm}^{-1}$ ). Phase cycling:  $\phi = x, -x$ ;  $\phi_{\text{rec}} = x, -x$  for axial peak suppression, and quadrature detection in  $t_1$  is accomplished by altering the phases  $\phi$  and  $\phi_{\text{rec}}$  according to the States-TPPI method.<sup>[27]</sup> A) Pulse scheme of SS simultaneous  $^{13}\text{C}^{\text{methyl}}/^{15}\text{N}-^1\text{H}$  HMQC. The delay  $d_2$  is set to a compromise value of 4.54 ms considering that  $^1J_{\text{CH}} \sim 125 \text{ Hz}$  and  $^1J_{\text{HN}} \sim 90 \text{ Hz}$ . Due to simultaneous decoupling of  $^{15}\text{N}$  and  $^{13}\text{C}$ , the maximum feasible duty cycle of the experimental set-up was reached at a minimal relaxation delay between scans of  $d_1 = \sim 150 \text{ ms}$  when  $t_{2,\text{max}} \sim 80 \text{ ms}$  (resulting in a delay of  $\sim 930 \text{ ms}$  between the acquisition of FIDs for each of the four slices). B) Pulse scheme of SS CT  $^{13}\text{C}^{\text{methyl}}-^1\text{H}$  HMQC with  $d_2 = 1/(2 J_{\text{CH}}) = 4.0 \text{ ms}$  and the CT delay  $d_3 = 28.0 \text{ ms}$ .<sup>[15]</sup> The maximum feasible duty cycle was reached at  $d_1 = \sim 100 \text{ ms}$  when  $t_{2,\text{max}} \sim 80 \text{ ms}$  (resulting in an effective delay of  $\sim 720 \text{ ms}$  between the acquisition of FIDs for each of the four slices).

FID of conventional HMQC while preserving the relaxation delay of the conventional experiment. Dividing the  $S/N$  ratio by the square root of the measurement time yields  $S/Nt$ , a measure of “intrinsic sensitivity”. If  $nt_{\text{SS}}$  and  $nt_{\text{C}}$  FIDs are acquired during the same time for SS and conventional HMQC, respectively,  $S/Nt_{\text{SS}}/S/Nt_{\text{C}}$  scales according to Equation (1):

$$\frac{S/Nt_{\text{SS}}}{S/Nt_{\text{C}}} \sim \left(\frac{\Delta z}{l}\right) \sqrt{\frac{nt_{\text{SS}}}{nt_{\text{C}}}} \quad (1)$$

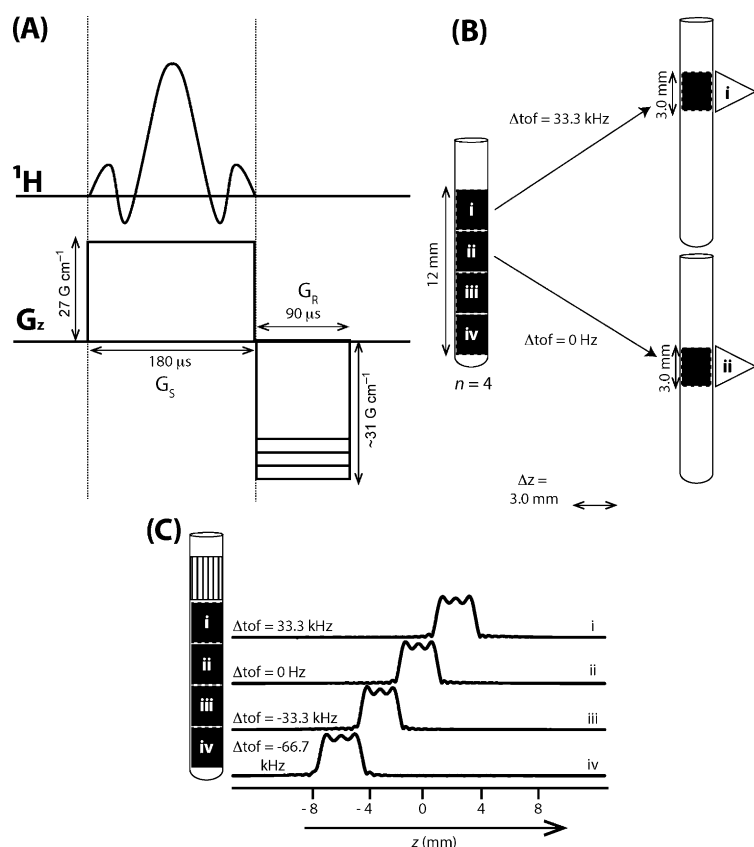


**Figure 3.** Implementation of SS excitation for HMQC with  $n=4$  slices (Figure 2) on a Varian INOVA 750 spectrometer equipped with a cryogenic  $^1\text{H}[^{13}\text{C},^{15}\text{N}]$  probe. A) Three-lobe sinc pulse of  $180\ \mu\text{s}$  duration applied along with a slice selection gradient  $G_s$  ( $27\ \text{G cm}^{-1}$ ) to excite a slice of  $3.0\ \text{mm}$  which is followed by a re-phasing gradient  $G_R$  ( $-31\ \text{G cm}^{-1}$ ) of opposite sign to compensate for the “phase ramp” along the slice that arises from the application of the sinc pulse. B) Four slices (i–iv) are depicted along  $12\ \text{mm}$  of the sample volume within the receiver coil to exemplify the required change of the offset,  $\Delta\text{tof}$ , from the  $^1\text{H}$  carrier frequency chosen for slice ii when exciting slice i. C) Spatial excitation profiles (right) for the slices (left) obtained by applying the sinc pulse and PFG depicted in (A), detecting the water  $^1\text{H}$  signal in the presence of a read-out PFG ( $3\ \text{G cm}^{-1}$ ), and subsequent Fourier transformation. Inspection of SS 1D  $^1\text{H}$  NMR spectra revealed that the top  $\sim 4\ \text{mm}$  section (hatched) could not be used for SS NMR (see the main text). Hence, four slices of  $3.0\ \text{mm}$  each were chosen as depicted while the top  $4\ \text{mm}$  of the sample volume within the RF coil could not be used.

Hence, if  $nt_{\text{SS}} = n \cdot nt_{\text{C}}$  (i.e. SS and conventional HMQC are acquired over the same total time) and the  $n$  slices cover the entire volume within the detection coil (i.e.  $n = l/\Delta z$ ),  $SNt_{\text{SS}}$  is lowered by  $1/\sqrt{n}$  compared to  $SNt_{\text{C}}$ . A further sensitivity loss results from the reduced efficiency of SS excitation when compared to excitation with a nonselective (high power) pulse,  $\varepsilon$ , which is  $\sim 0.80$  for the selective pulse used for the implementation<sup>[11]</sup> described here (Figure 3).

Moreover,  $T_1$  relaxation should be considered. In particular, such relaxation occurs in SS HMQC between the two nonselective  $180^\circ\ ^1\text{H}$  pulses (Figure 4) outside of the excited slice, which leads to additional reduction of the detected signal intensity:  $^1\text{H}$  magnetization is flipped to  $-z$  and back to  $+z$  for  $n-1$  times between detection of two subsequent FIDs for a given slice.

For non-CT experiments, the resulting loss of detected signal is also a function of  $t_1$  and thus leads, even for a comparably short  $^1\text{H}$   $T_1$  of  $500\ \text{ms}$ , to a very small signal broadening ( $< \sim 1\ \text{Hz}$ ; Fig-

ure S2) along the indirect dimension (see the Supporting Information). With  $m_k = M_{z,k}/M_z^{\text{eq}}$  corresponding to the magnetization along the  $z$  axis at time point  $k$  divided by its equilibrium value and considering mono-exponential  $T_1$  relaxation during a delay  $\tau$  between time points  $k$  and  $k+1$  (during which no RF pulses are applied), one can derive Equation (2):

$$m_{k+1} = 1 + (m_k - 1) \exp\left(-\frac{\tau}{T_1}\right) \quad (2)$$

A formula was thus derived (see the Supporting Information) for the ratio  $\rho$  of the  $^1\text{H}$  steady-state magnetizations present before the first  $90^\circ\ ^1\text{H}$  pulse in a given slice of SS and in conventional HMQC experiments. Using Equation (2), the steady-state magnetizations  $m_{\text{SS}}$  and  $m_{\text{C}}$  present in a given slice in SS HMQC acquired with four slices and in conventional HMQC, respectively, are [see the Supporting Information and Equations (3) and (4)]:

$$m_{\text{SS}} = 1 + 2 \sum_{i=0,1,2,3} B^{i+1} (A^{i+1} - A^i) - A^4 B^4 \quad (3)$$

$$m_{\text{C}} = 1 - 2B + AB \quad (4)$$

where:

$$A = \exp\left(-\frac{\tau_1}{T_1}\right) \text{ and } B = \exp\left(-\frac{\tau_2}{T_1}\right)$$

where  $\tau_1$  and  $\tau_2$  (e.g.  $4.54$  and  $233.54\ \text{ms}$  for both SS and conventional HMQC at  $t_1 = 0\ \text{ms}$  in this study) are, respectively, the delays before and after the application of the  $^1\text{H}$   $180^\circ$  refocusing pulses (during which relaxation is neglected). Dividing Equation (3) by Equation (4) yields the desired ratio  $\rho$  [Eq. (5)]:

$$\rho = \frac{m_{\text{SS}}}{m_{\text{C}}} \quad (5)$$

After multiplication of  $\rho$  with  $\varepsilon$  and  $(\Delta z/l)(nt_{\text{SS}}/nt_{\text{C}})^{1/2}$  in Equation (1), the ratio of the corresponding  $SN_t$  values is obtained [Eq. (6)]:

$$\frac{SNt_{\text{SS}}}{SNt_{\text{C}}} = \rho \times \varepsilon \times \left(\frac{\Delta z}{l}\right) \sqrt{\frac{nt_{\text{SS}}}{nt_{\text{C}}}} \quad (6)$$

Figure 5 provides a plot of  $SNt_{\text{SS}}/SNt_{\text{C}}$  versus  $^1\text{H}$   $T_1$  for  $\Delta z/l = 3/16$  (solid line; for present study, see Figure 3); and for  $\Delta z/l = 1/4$  (dashed line; if the whole sample volume within the RF coil can be used for SS NMR),  $\varepsilon = 0.80$ , and  $t_1 = 0\ \text{ms}$  and  $nt_{\text{SS}} = nt_{\text{C}}$  that is, for data acquired rapidly with identical sampling speed (relaxation delay between scans  $d_1 = 150\ \text{ms}$  for both SS and conventional HMQC; Table S1). Inspection of Figure 5 reveals (i) that for short  $T_1$  the ratio increases largely with  $T_1$  (which reflects the four times longer effective inter-scan delays,  $d_1 + t_{2,\text{max}}$  in SS HMQC), and (ii) that for  $T_1$  around  $1.5\ \text{s}$  the intrinsic sensitivity of SS NMR can be expected to be, respectively, about  $50\%$  and  $70\%$  of the sensitivity of conventional HMQC for  $\Delta z/l = 3/16$  and  $\Delta z/l = 1/4$  (whole sample volume available for SS NMR).

In principle, the translational diffusion of protein molecules needs to be considered to assess the intrinsic sensitivity of SS NMR. For the current implementation of SS NMR, however, a nonselective  $180^\circ\ ^1\text{H}$  pulse is applied for the refocusing of transverse  $^1\text{H}$  mag-

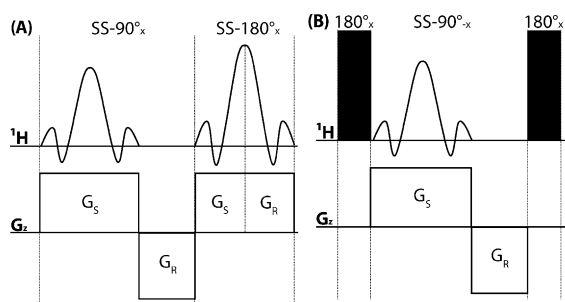


**Figure 4.** Conceptual comparison of two conceivable implementations of SS HMQC with  $n=4$  slices. A) Hypothetical implementation in which both the  $90^\circ$  excitation pulse and the  $180^\circ$  pulse for refocusing  $^1\text{H}$  chemical shift evolution are SS. As a result, the steady-state magnetization of only one selected slice is converted into transverse magnetization (as shown on the right). Large sensitivity losses result from the second SS pulse. B) The implementation in this study, in which a nonselective  $180^\circ$  pulse is applied first to invert the longitudinal magnetization of the entire sample, followed by a selective  $90^\circ$  pulse to excite a selected slice and then a nonselective  $180^\circ$  pulse for refocusing  $^1\text{H}$  chemical shift evolution which also returns longitudinal magnetization to  $+z$  in the slices that are not excited.

netization during the indirect evolution period along with nonselective heteronuclear  $90^\circ$  pulses (Figure 2). As a result, protein molecules diffusing outside of the excited slice, while remaining within the receiver coil during the time elapsed between slice-selective excitation and signal detection, still contribute to the signal (which is detected over the entire sample volume). Furthermore, the diffusion coefficient  $D$ , even for the small (7.6 kDa) protein ubiquitin ( $1.3 \times 10^{-4} \text{ mm}^2 \text{ s}^{-1}$  at  $25^\circ\text{C}$ ), results in a root-mean-squared displacement ( $\sqrt{2Dt}$ ) of only  $\sim 16 \mu\text{m}$  when the delays between excitation and signal detection are shorter than 1 s. Hence, translational diffusion does not result in any noticeable loss of sensitivity in SS HMQC experiments.

## 2. Results and Discussion

First, SS HMQC experiments were implemented and optimized using the sample containing the 7.6 kDa protein ubiquitin (3.7 mM). To demonstrate the impact of time-staggered data acquisition (Figure 1), the average  $S/N$  was measured as a function of the inter-scan delay and then compared with conventional HMQC acquired using the same sampling speed.  $S/N$  ratios were normalized relative to the values observed for (nearly) fully relaxed  $^1\text{H}$  spins at very long relaxation delays (Figure 6). Because the relaxation delay between two FIDs recorded from each of the four slices in SS HMQC is four times longer than the delay between two consecutive FIDs recorded in conventional HMQC (Figure 1), the  $S/N$  ratios increase, as expected, about four times faster for SS HMQC (Figure 6).

Second, SS HMQC spectra were acquired with relaxation delays  $d_1$  of 150 and 100 ms between scans for sim and CT-HMQC, respectively, for the three proteins with varying molecular weights and  $^1\text{H}$   $T_1$  relaxation times (Table S1), namely, U- $^{13}\text{C},^{15}\text{N}$  ubiquitin (7.6 kDa), and the two U- $^{2}\text{H},^{13}\text{C},^{15}\text{N}$ -labeled, ILV methyl protonated proteins GmR137 (7.5 kDa) and MBP (43.4 kDa). For comparison, conventional HMQC spectra were recorded with the same relaxation delays and measurement times. One set of HMQC spectra was acquired with comparably long measurement times (6–24 min; Table S1) to ensure that  $S/N > \sim 30$  for all peaks, in order to compare accurately the intrinsic sensitivity of SS and conventional HMQC.  $S/N_{\text{SS}}/S/N_{\text{C}}$  was calculated for well-resolved peaks and the resulting averages and ranges are shown along with the corresponding averages and ranges of  $^1\text{H}$   $T_1$  relaxation times (Table S1) in Figure 5. The close agreement with predictions based on Equation (6) neatly validates the expected performance of the implementation of SS HMQC reported here (Figure 2). A second set of spectra was acquired with short measurement times of 45–120 s to demon-

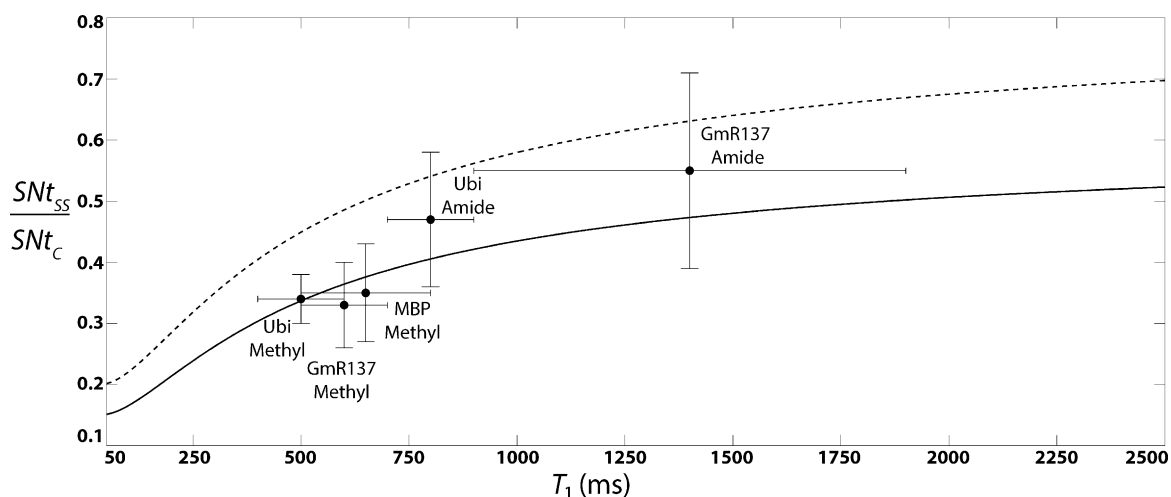


**Figure 5.** The ratio of the intrinsic sensitivities of SS HMQC with  $n=4$  slices,  $S/N_{\text{SS}}$ , and conventional HMQC,  $S/N_{\text{C}}$ , calculated according to Equation (6), is plotted (solid line) versus  $^1\text{H}$   $T_1$  relaxation times for identical sampling speed ( $nt_{\text{SS}} = nt_{\text{C}}$ ) at  $t_1 = 0$  ms, and with  $\Delta z/l = 3/16$  and an inter-scan delay of 230 ms. Also shown are experimental values obtained for three protein samples (see the main text for details; Ubi: ubiquitin). The bars indicate the ranges that were measured for  $^1\text{H}$   $T_1$  and  $S/N$  values. For comparison,  $S/N_{\text{SS}}/S/N_{\text{C}}$  is also plotted (dashed line) for  $\Delta z/l = 1/4$  to illustrate the loss of sensitivity resulting from hardware limitations of our spectrometer (Figure 3), specifically the fact that the top 4 mm of the sample could not be used for SS NMR (see the main text).  $S/N$  values were calculated by dividing signal intensities by 2.5 times the standard deviation of the noise as measured in noise regions of the 2D spectra.

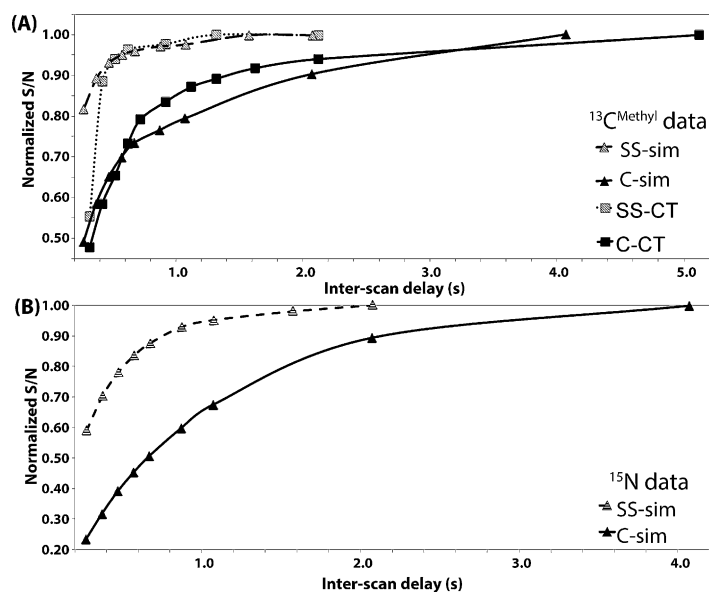


**Figure 6.** Average  $S/N$  ratios measured for signals in spectra recorded for ubiquitin were normalized by dividing them with the  $S/N$  ratio observed at long delays between the acquisition of FIDs ("inter-scan delays") and then plotted versus the inter-scan delay. C: conventional HMQC. A) Methyl signals. B) Polypeptide backbone amide signals.

strate the feasibility of rapid data acquisition ( $S/N > 10$  for all peaks). Likewise, high-quality SS HMQC spectra (Figure 7) were obtained and 96–100% of the peaks detected in conventional HMQC spectra (Figure S4) were registered.

### 3. Conclusions

The developments described here make SS HMQC a valuable addition to the portfolio of experiments for obtaining 2D NMR spectral information rapidly. Importantly, time-staggered acquisition enables one to employ long relaxation delays at high repetition rates. This acquisition scheme promises to be particularly valuable for systems with long  $T_1$  relaxation times and/or for NMR experiments for which short relaxation delays can impede data analysis. For example, cross peaks in  $^1\text{H}$ – $^1\text{H}$  NOESY depend on the steady-state magnetization of dipolar-coupled protons (so that upper distance limit constraints derived from spectra recorded with short relaxation delay are inaccurate). Notably, band-selective optimized-flip-angle short-transient (SOFAST)  $^{15}\text{N}$ – $^1\text{H}$  HMQC<sup>[4f]</sup> relies on L-optimization<sup>[9]</sup> to accelerate sampling speed.<sup>[2a,6b,16]</sup> Hence, in contrast to the SS HMQC experiments presented here, SOFAST HMQC 1) does not

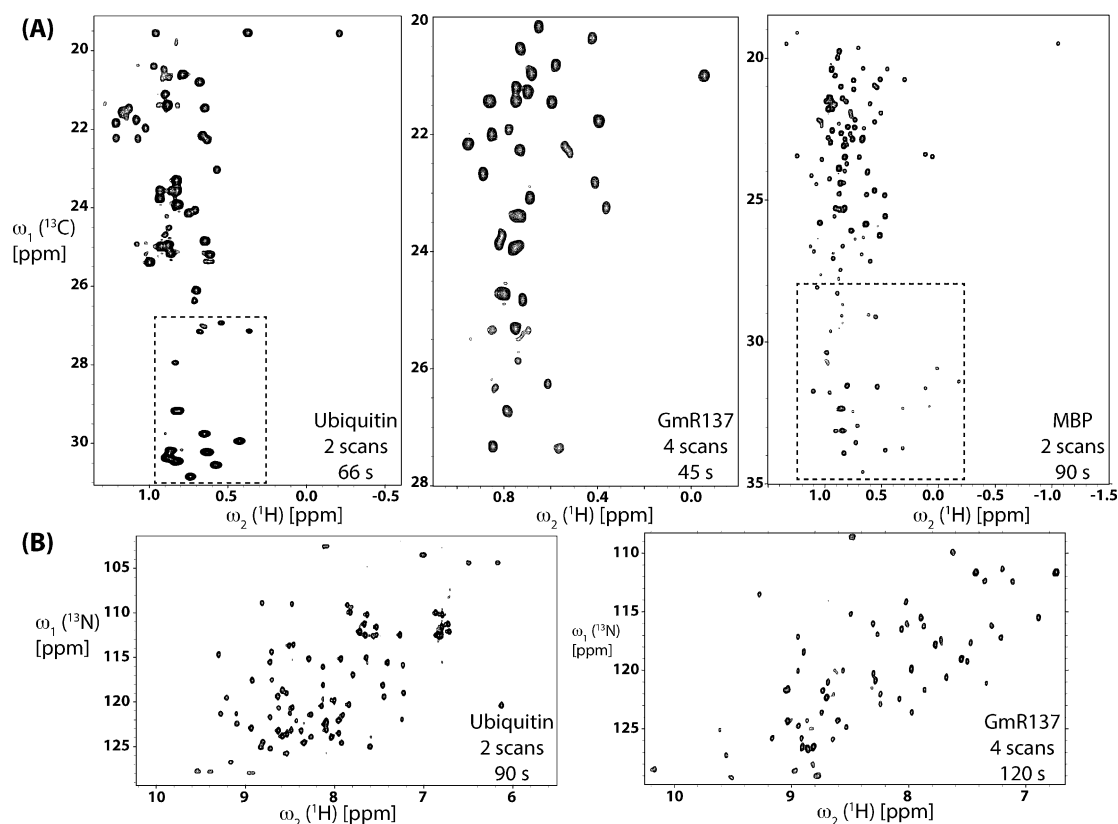


**Figure 7.** Rapidly acquired SS HMQC spectra (for acquisition parameters, see Table S1). A) SS CT-HMQC spectra collected over 66 s for ubiquitin, 45 s for GmR137 and 90 s for MBP (boxed spectral regions contain folded peaks). B) Spectral regions containing polypeptide backbone NH signals of sim-HMQC spectra acquired over 90 s for ubiquitin and 120 s for GmR137.

use long relaxation delays between scans, 2) cannot be considered for simultaneous  $^{13}\text{C}^{\text{methyl}}/^{15}\text{N}^{-1}\text{H}$  HMQC data acquisition, and 3) is of limited use for deuterated proteins. Moreover, SS simultaneous  $^{13}\text{C}^{\text{aromatic}}/^{15}\text{N}^{-1}\text{H}$  HMQC could be readily implemented for the study of aromatic rings, as a valuable probe of protein structure and dynamics.<sup>[29]</sup> We thus expect that SS and SOFAST HMQC will be complementary techniques for use in future biomolecular studies.

Importantly, SS NMR can be readily combined with other approaches for rapid data acquisition such as SC NMR,<sup>[11]</sup> Hadamard NMR,<sup>[10]</sup> as well as non-uniform time domain sampling schemes<sup>[6]</sup> including GFT NMR.<sup>[6]</sup> In particular, SC NMR could be used to implement a minimal two-step phase cycle for axial peak suppression and combined with SS NMR for quadrature detection, potentially in clean absorption mode to remove residual phase errors.<sup>[30]</sup> Similarly, SS NMR might be a viable option for recording spectra more rapidly to obtain relative concentrations of compounds, for example, when measuring kinetic isotope effects,<sup>[31]</sup> which depends on exciting largely relaxed spin systems. Finally, it is conceivable to develop multi-element receiver coils that might render SS NMR intrinsically more sensitive than conventional HMQC (noise arising from non-excited slices could be excluded during signal detection), and also to extend the SS NMR approach to volume-selective excitation using triple-axis gradient probes.

## Acknowledgements

This work was supported by the National Science Foundation (MCB 0817857 to T.S.) and the National Institutes of Health (GM094597 to G.T.M.). We thank Dr. Dinesh Sukumaran for helpful discussions.

**Keywords:** flip-back pulses · HMQC · rapid data acquisition · spatially selective NMR · time-staggered data acquisition

- [1] H. Kovacs, D. Moskau, M. Spraul, *Prog. Nucl. Magn. Reson. Spectrosc.* **2005**, *46*, 131–155.
- [2] a) H. S. Atreya, T. Szyperski, *Methods Enzymol.* **2005**, *394*, 78–108; b) I. C. Felli, B. Brutscher, *ChemPhysChem* **2009**, *10*, 1356–1368; c) T. Szyperski, G. T. Montelione in *Biomolecular NMR Spectroscopy*, Vol. 3 (Eds.: A. J. Dingley, S. M. Pascal), IOS Press, Amsterdam, **2011**, pp. 366–380; d) E. Rennella, B. Brutscher, *ChemPhysChem* **2013**, *14*, 3059–3070.
- [3] a) G. T. Montelione, C. Arrowsmith, M. Girvin, M. Kennedy, J. Markley, R. Powers, J. Prestegard, T. Szyperski, *J. Struct. Funct. Genomics* **2009**, *10*, 101–106; b) G. T. Montelione, T. Szyperski, *Curr. Opin. Drug Discovery Dev.* **2010**, *13*, 335–349.
- [4] a) L. Frydman, T. Scherf, A. Lupulescu, *Proc. Natl. Acad. Sci. USA* **2002**, *99*, 15858–15862; b) L. Frydman, A. Lupulescu, T. Scherf, *J. Am. Chem. Soc.* **2003**, *125*, 9204–9217; c) P. Schanda, E. Kupce, B. Brutscher, *J. Biomol. NMR* **2005**, *33*, 199–211; d) P. Schanda, B. Brutscher, *J. Am. Chem. Soc.* **2005**, *127*, 8014–8015; e) P. Schanda, B. Brutscher, *J. Magn. Reson.* **2006**, *178*, 334–339; f) P. Schanda, H. Van Melckebeke, B. Brutscher, *J. Am. Chem. Soc.* **2006**, *128*, 9042–9043; g) P. Schanda, V. Forge, B. Brutscher, *Magn. Reson. Chem.* **2006**, *44*, S177–S184; h) P. Schanda, V. Forge, B. Brutscher, *Proc. Natl. Acad. Sci. USA* **2007**, *104*, 11257–11262; i) M. Gal, P. Schanda, B. Brutscher, L. Frydman, *J. Am. Chem. Soc.* **2007**, *129*, 1372–1377; j) T. Kern, P. Schanda, B. Brutscher, *J. Magn. Reson.* **2008**, *190*, 333–338; k) C. Amero, P. Schanda, M. A. Dura, I. Ayala, D. Marion, B. Franzetti, B. Brutscher, J. Boisbouvier, *J. Am. Chem. Soc.* **2009**, *131*, 3448–3449; l) M. Gal, T. Kern, P. Schanda, L. Frydman, B. Brutscher, *J. Biomol. NMR* **2009**, *43*, 1–10; m) A. Corazza, E. Rennella, P. Schanda, M. C. Mimmi, T. Cutuil, S. Raimondi, S. Giorgetti, F. Fogolari, P. Viglino, L. Frydman, M. Gal, V. Bellotti, B. Brutscher, G. Esposito, *J. Biol. Chem.* **2010**, *285*, 5827–5835; n) Y. Shrot, L. Frydman, *J. Magn. Reson.* **2011**, *209*, 352–358; o) E. Rennella, T. Cutuil, P. Schanda, I. Ayala, V. Forge, B. Brutscher, *J. Am. Chem. Soc.* **2012**, *134*, 8066–8069; p) P. E. S. Smith, K. J. Donovan, O. Szekely, M. Baias, L. Frydman, *ChemPhysChem* **2013**, *14*, 3138–3145.
- [5] a) T. Szyperski, G. Wider, J. H. Bushweller, K. Wuethrich, *J. Am. Chem. Soc.* **1993**, *115*, 9307–9308; b) T. Szyperski, D. C. Yeh, D. K. Sukumaran, H. N. B. Moseley, G. T. Montelione, *Proc. Natl. Acad. Sci. USA* **2002**, *99*, 8009–8014.
- [6] a) S. Kim, T. Szyperski, *J. Am. Chem. Soc.* **2003**, *125*, 1385–1393; b) H. S. Atreya, T. Szyperski, *Proc. Natl. Acad. Sci. USA* **2004**, *101*, 9642–9647; c) H. S. Atreya, A. Eletsy, T. Szyperski, *J. Am. Chem. Soc.* **2005**, *127*, 4554–4555; d) H. S. Atreya, E. Garcia, Y. Shen, T. Szyperski, *J. Am. Chem. Soc.* **2007**, *129*, 680–692; e) H. S. Atreya, B. Sathyamoorthy, G. Jaipuria, V. Beaumont, G. Varani, T. Szyperski, *J. Biomol. NMR* **2012**, *54*, 337–342.
- [7] a) E. Kupce, R. Freeman, *J. Am. Chem. Soc.* **2004**, *126*, 6429–6440; b) S. Hiller, F. Fiorito, K. Wuethrich, G. Wider, *Proc. Natl. Acad. Sci. USA* **2005**, *102*, 10876–10881.
- [8] M. Mobli, M. W. Maciejewski, A. D. Schuyler, A. S. Stern, J. C. Hoch, *Phys. Chem. Chem. Phys.* **2012**, *14*, 10835–10843.
- [9] K. Pervushin, B. Vögeli, A. Eletsy, *J. Am. Chem. Soc.* **2002**, *124*, 12898–12902.
- [10] E. Kupče, R. Freeman, *J. Magn. Reson.* **2003**, *163*, 56–63.
- [11] D. M. Parish, T. Szyperski, *J. Am. Chem. Soc.* **2008**, *130*, 4925–4933.
- [12] J. Cavanagh, W. J. Fairbrother, A. G. Palmer III, M. Rance, N. J. Skelton, *Protein NMR Spectroscopy 2nd ed.*, Elsevier, Amsterdam, **2007**.
- [13] a) M. Vega-Vazquez, J. C. Cobas, M. Martin-Pastor, *Magn. Reson. Chem.* **2010**, *48*, 749–752; b) N. Giraud, L. Beguin, J. Courtieu, D. Merlet, *Angew. Chem.* **2010**, *122*, 3559–3562; *Angew. Chem. Int. Ed.* **2010**, *49*, 3481–3484.
- [14] R. Bhattacharyya, A. Kumar, *Chem. Phys. Lett.* **2004**, *383*, 99–103.
- [15] M. J. Thrippleton, N. M. Loening, J. Keeler, *Magn. Reson. Chem.* **2003**, *41*, 441–447.
- [16] a) A. Eletsy, H. S. Atreya, G. Liu, T. Szyperski, *J. Am. Chem. Soc.* **2005**, *127*, 14578–14579; b) M. Deschamps, I. D. Campbell, *J. Magn. Reson.* **2006**, *178*, 206–211.
- [17] R. R. Ernst, G. Bodenhausen, A. Wokaun, *Principles of Nuclear Magnetic Resonance in One and Two Dimensions*, Oxford University Press, London, **1987**.
- [18] K. Lu, X. Heng, L. Garyu, S. Monti, E. L. Garcia, S. Kharytonchyk, B. Dorj-suren, G. Kulandaivel, S. Jones, A. Hiremath, S. S. Divakaruni, C. LaCotti, S. Barton, D. Tummillo, A. Husic, K. Edme, S. Albrecht, A. Telesnitsky, M. F. Summers, *Science* **2011**, *334*, 242–245.
- [19] a) L. Mueller, *J. Am. Chem. Soc.* **1979**, *101*, 4481–4484; b) A. Bax, R. H. Griffey, B. L. Hawkins, *J. Magn. Reson.* **1983**, *55*, 301–315.
- [20] a) B. Farmer II, L. Mueller, *J. Biomol. NMR* **1994**, *4*, 673–687; b) S. M. Pascal, D. R. Muhandiram, T. Yamazaki, J. D. Formankay, L. E. Kay, *J. Magn. Reson. Ser. B* **1994**, *103*, 197–201; c) D. Uhrin, J. Bramham, S. Winder, P. Barlow, *J. Biomol. NMR* **2000**, *18*, 253–259; d) Y. Xia, A. Yee, C. Arrowsmith, X. Gao, *J. Biomol. NMR* **2003**, *27*, 193–203; e) Y. Shen, H. S. Atreya, G. Liu, T. Szyperski, *J. Am. Chem. Soc.* **2005**, *127*, 9085–9099; f) T. Parella, P. Nolis, *Concept Magnetic Res.* **2010**, *36A*, 1–23.
- [21] a) J. Santoro, G. C. King, *J. Magn. Reson.* **1992**, *97*, 202–207; b) G. W. Vuister, A. Bax, *J. Magn. Reson.* **1992**, *98*, 428–435.
- [22] A. Ruschak, L. Kay, *J. Biomol. NMR* **2010**, *46*, 75–87.
- [23] J. E. Ollershaw, V. Tugarinov, L. E. Kay, *Magn. Reson. Chem.* **2003**, *41*, 843–852.
- [24] O. F. Lange, P. Rossi, N. G. Sgourakis, Y. Song, H.-W. Lee, J. M. Aramini, A. Ertekin, R. Xiao, T. B. Acton, G. T. Montelione, D. Baker, *Proc. Natl. Acad. Sci. USA* **2012**, *109*, 10873–10878.
- [25] F. Delaglio, S. Grzesiek, G. W. Vuister, G. Zhu, J. Pfeifer, A. Bax, *J. Biomol. NMR* **1995**, *6*, 277–293.
- [26] A. J. Shaka, P. B. Barker, R. Freeman, *J. Magn. Reson.* **1985**, *64*, 547–552.
- [27] D. Marion, M. Ikura, R. Tschudin, A. Bax, *J. Magn. Reson.* **1989**, *85*, 393–399.
- [28] M. Bernstein, K. King, X. Zhou, *Handbook of MRI Pulse Sequences: A Guide for Scientists, Engineers, Radiologists, Technologists*, Elsevier Academic Press, Burlington, **2004**, pp. 38–41.

- [29] a) J. J. Skalicky, J. L. Mills, S. Sharma, T. Szyperki, *J. Am. Chem. Soc.* **2001**, *123*, 388–397; b) B. Sathyamoorthy, K. K. Singarapu, A. E. Garcia, T. Szyperki, *ChemBioChem* **2013**, *14*, 684–688.
- [30] a) Y. Wu, A. Ghosh, T. Szyperki, *Angew. Chem.* **2009**, *121*, 1507–1511; *Angew. Chem. Int. Ed.* **2009**, *48*, 1479–1483; b) Y. Wu, A. Ghosh, T. Szyperki, *J. Struct. Funct. Genomics* **2009**, *10*, 227–232; c) A. Ghosh, Y. Wu, Y. He, T. Szyperki, *J. Magn. Reson.* **2011**, *213*, 46–57.
- [31] K. A. Manning, B. Sathyamoorthy, A. Eletsy, T. Szyperki, A. S. Murkin, *J. Am. Chem. Soc.* **2012**, *134*, 20589–20592.

---

Received: December 30, 2013

Published online on April 30, 2014